Superfast Proton Diffusion Achieved in a Plasma-Polymerized Fuel- Cell Membrane

DATASET *in* THE JOURNAL OF PHYSICAL CHEMISTRY C · FEBRUARY 2013

Impact Factor: 4.77 · DOI: 10.1021/jp309259k

5 AUTHORS, INCLUDING:

Cormac Corr
Australian National University
86 PUBLICATIONS **509** CITATIONS
SEE PROFILE

Zunbeltz Izaola
European Spallation Source Bilbao
29 PUBLICATIONS **123** CITATIONS
SEE PROFILE

THE JOURNAL OF PHYSICAL CHEMISTRY C

Article

pubs.acs.org/JPCC

Superfast Proton Diffusion Achieved in a Plasma-Polymerized Fuel-Cell Membrane

Vanessa K. Peterson,*[,†] Cormac S. Corr,[‡] Roderick W. Boswell,[‡] Zunbeltz Izaola,[§,∥] and Gordon J. Kearley[†]

[†]Australian Nuclear Science and Technology Organisation, Lucas Heights, NSW, Australia

[‡]Research School of Physics and Engineering, Australian National University, Canberra, ACT, Australia

[§]Berlin Neutron Scattering Center, Helmholtz Zentrum Berlin für Materialien und Energie, Berlin, Germany

Supporting Information

ABSTRACT: We measure superfast proton diffusion in a proton-exchange membrane (PEM) produced by plasma polymerization. The proton self-diffusion is measured in water-saturated PEMs from the proton autocorrelation function obtained from quasielastic neutron scattering (QENS). 41(3)% of protons in the plasma-produced membrane diffuse at a rate that is an order of magnitude faster than that measured in the commercially available membrane, Nafion, and this is achieved in low hydration conditions. Both molecular dynamic simulations and experimental results are consistent with an assisted superfast diffusion process that may open the way to more powerful fuel cells.

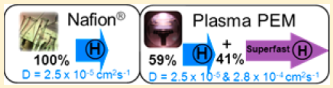

INTRODUCTION

Proton-exchange membrane (PEM) fuel cells are among key enabling technologies for zero-emission vehicles.[1] The polymer membranes possess covalently linked acidic functionalities that permit protons to pass directly to the cathode, while forcing the electrons through a circuit. The amount of electricity produced by the fuel cell is directly proportional to the transport of protons across the membrane. Commercially available chemically prepared ion-exchange membranes such as Nafion are based on a hydrophobic tetrafluoroethylene backbone polymer with pendant side chains terminating with hydrophilic sulfonic acid groups.[2] Nafion membranes have a microscopically phase-separated structure in which it is difficult to improve proton conduction. One way of addressing this is to prepare perfluorinated ion-exchange membranes with a highly cross-linked structure, providing the opportunity to enhance ion-exchange capacity.[3,4] Plasma polymerization can be used to create amorphous three-dimensional membranes that are cross-linked, thin, and dense.

The chemical composition and microstructural characteristics such as morphology of plasma-polymerized membranes can be directly and rapidly controlled over a wide range by changing the plasma parameters such as discharge power, gas pressures, flow rates, and substrate bias.[4] Furthermore, the pulsed-plasma technique can be used to control the growth process and to obtain the desired film structure and uniformity.[4] This approach has two distinct reaction regimes: the first corresponding to the duty cycle on-period, which generates active sites (via ultraviolet irradiation, ion, or electron bombardment), followed by the second regime corresponding to conventional polymerization, occurring during the off-period (in the absence of any radiation, ion, or electron-induced damage) and enabling controlled layer mechanism growth. This gives rise to structural retention in conjunction with the incorporation of specific functional groups.[5−7] The plasma-polymerization method has additional advantages that include ease of thickness control during the deposition process, the strong adhesion of the membrane onto substrates such as electrodes and conformal coatings, and good chemical and thermal stability enabled by the cross-linked structure.[4] In particular, the controllable degree of cross-linking achievable in plasma polymerization enables adjustment of mechanical properties and is expected to lead to increased degradation resistance. Using this approach, it should be possible to obtain highly conductive membranes that have increased chemical and thermal stability, leading to a longer lifetime and ability to operate at temperatures greater than 100 °C without the need for external humidification of the reactant gases. The ease of thickness control during the deposition process also affords miniaturization, which is a feature that revolutionized the microelectronics industry. Plasma polymers are clearly attractive for fuel cells.

Studies of the dynamics of protons in the membrane are key to understanding the proton transport mechanism and of great importance to the development of new PEM materials. Accordingly, proton transport in Nafion has been extensively studied, with significant contributions made through studies of proton self-diffusion.[2] Despite the attractiveness for fuel cells, there has been little work studying proton-transport through plasma polymerized membranes. This is perhaps even more surprising given that plasma-produced PEMs (PP-PEMs) can have higher proton conductivities than Nafion,[8−10] and the reasons for this are currently unknown. Variations in plasma conditions affect the incorporation of ion-exchange groups into

Received: September 18, 2012
Revised: January 31, 2013
Published: February 14, 2013

the membrane, with a variety of measured proton conductivities of PP-PEMs measured, relative to Nafion.[3,4,8−10] Proton conductivity differs from proton self-diffusion, with the former giving little detail concerning the diffusion mechanism of the protons and often indirectly measured from the electrical response of a system using impedance spectroscopy. While the Nernst−Einstein relation can be used to obtain an effective diffusion coefficient from impedance spectroscopy data if the proton concentration is known, this coefficient is not comparable with the chemical diffusion coefficient obtained using methods such as QENS, with the driving force for the particle being the electric field rather than the gradient of the chemical potential (changing chemical potential). Further, unlike QENS, impedance spectroscopy is unable to determine fast processes like strongly localized motions of the protons.

Studies of proton self-diffusion via measurement of the proton autocorrelation function using QENS have yielded information on both the self-diffusion constant (diffusion rate) and the geometry of proton motion (diffusion type) in Nafion.[11−17] Further, QENS quantitatively distinguishes between protons with different types of diffusion that are simultaneously present. Such studies applied to PP-PEMs may unlock the link between the proton motions that give rise to favorable proton conductivities, with such insights enabling the chemical engineering of membranes to optimize PEM performance.

In a QENS experiment, the scattered neutrons may exchange some energy with the moving nuclei (including the protons) that comprise the sample, directly measuring their movement. QENS data, $S(Q,\omega)$, are a function of the scattering vector (Q), a measure of reciprocal length in the material, and the neutron-energy transfer ($h/2\omega\pi$, where h is Planck's constant), a measure of dynamics. Analysis of the energy exchange between the neutrons and the sample and the scattering vector of the neutrons in an experiment gives information concerning the motions of the nuclei, including their time scale and geometry. QENS data, $S(Q,\omega)$, therefore report the probability that a proton is within a given range of its original position as a function of time, allowing direct measurement of proton self-diffusion.

The proton conductivity (measured through impedance spectroscopy) of the PP-PEMS studied here, produced from styrene and trifluoromethanesulfonic acid, is ∼21% higher than that for Nafion,[8−10] and our QENS study reveals that 41(3)% of the protons in the PP-PEM are undergoing diffusion with a self-diffusion constant that is an order of magnitude faster than in Nafion. Significantly, the QENS signal shows mechanistic differences in the proton motions, including their geometry, between the protons in Nafion and those in the PP-PEM that are moving much faster. We quantitatively derive these mechanistic differences between proton diffusion in Nafion and the superfast process in the PP-PEM.

EXPERIMENTAL METHODS

A pulsed-plasma enhanced chemical vapor-deposition (P-PECVD) system was developed within the Space Plasma, Power, and Propulsion (SP^3) group at The Australian National University to fabricate novel hydrogen-ion exchange membranes that can be used in PEM fuel cells. The plasma system consists of an upper part, where the plasma is created in a Pyrex tube (source), and the film deposition region in the lower part (deposition chamber), where the film precursors are introduced (Figure 1). In the inductively coupled plasma reactor a plasma

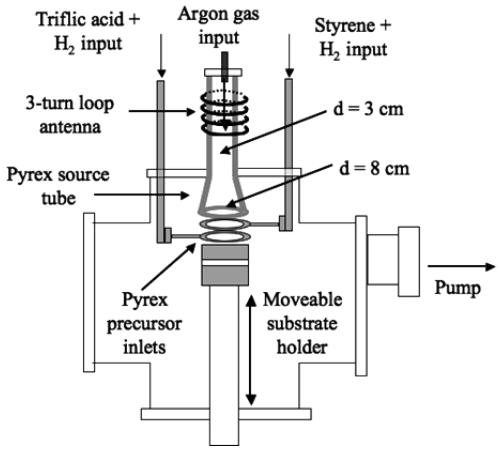

Figure 1. Schematic of the plasma polymerization system, where d is diameter.

discharge in the source is obtained by applying 13.56 MHz power to a three-turn copper antenna surrounding the source tube. This reactor can operate in both an inductive mode, with a high-plasma density (>10^{10} cm^{-3}), and a capacitive mode, with a low-plasma density (<10^{10} cm^{-3}), enabling high and low fragmentation of the precursors and different polymer membranes to be produced.

The plasma-processing system was operated in a pulsed-discharge mode (8 ms on and 60 ms off) in order to influence the gas-phase reactions of radicals and surface reactions of precursors. 100 μm thick PP-PEMs were fabricated on Al foil using a total pulse length of 68 ms and an 11.76% duty cycle, with a total process time of 10 min. The average power was 20 W.

Trifluoromethanesulfonic acid and styrene entered the deposition region via glass circular inlets. The acid was heated to 80 °C and the styrene to 40 °C, with H_2 as the carrier. The precursor flow was controlled using mass-flow controllers (0−10 sccm). Gas lines were heated to avoid polymerization and/or condensation of monomers on their walls. A butterfly valve placed between the deposition chamber and the vacuum pump controlled the pressure in the reactor at 80 Pa. Nafion 115 membranes were treated by immersion in H_2O_2 at 60 °C for 60 min, washed in deionized water, and then immersed in H_2SO_4 at 60 °C for 60 min, before being washed in deionized water and dried at 100 °C.

Neutron scattering measurements were performed using the treated Nafion and PP-PEMs which were cut to obtain 5 cm × 2 cm strips. Each strip was soaked in deionized water for 15 min (when saturation was achieved), wiped with filter paper, and wrapped around an aluminum insert placed inside an annular aluminum can sealed with an indium gasket. QENS data were collected using the NEAT (V3) instrument at the Berlin Neutron Scattering Center. Incident neutrons with a wavelength of 5.1 Å were used in an instrument configuration that gave ≈140 μeV energy resolution at the elastic line. Data were collected at 300 K over 8−13 h for the PP-PEMs and 1−2 h for the Nafion. The raw data were normalized to correct for variations in incident flux and in detector efficiency using data from a standard vanadium sample and summed over $\Delta Q = 0.12$ $Å^{-1}$ from $Q = 0.36-1.92$ $Å^{-1}$. The Nafion is perfluorinated while the PP-PEM is a hydrogenated membrane (see the high-resolution X-ray photoelectron spectra for carbon for the membranes, Figure S1). QENS data are dominated by

dx.doi.org/10.1021/jp309259k | J. Phys. Chem. C 2013, 117, 4351−4357

scattering from hydrogen nuclei, with the hydrogen nucleus (^{1}H) contributing ~40 times more to the QENS signal than the deuterium (^{2}H) nucleus. Therefore, the signal from the protons in the water added was separated from those in the membrane by obtaining spectra for samples hydrated with ^1H_2O and ^2H_2O:

$$S_{PEM+^1H_2O}(Q, \omega) = S_{PEM}(Q, \omega) + S_{^1H_2O}(Q, \omega)$$

$$S_{PEM+^2H_2O}(Q, \omega) = S_{PEM}(Q, \omega) + S_{^2H_2O}(Q, \omega)$$

$$S_{PEM+^1H_2O}(Q, \omega) - S_{PEM+^2H_2O}(Q, \omega) = S_{^1H_2O}(Q, \omega) - S_{^2H_2O}(Q, \omega) \quad (1)$$

The signal from the protons dominates the QENS data, regardless of other nuclei in the sample (including the aluminum substrate and sample container as well as the PEM components).

The ion-exchange capacity (IEC) was measured by soaking the dry PEM in 30 mL of saturated sodium chloride solution at room temperature for 48 h and titrating with a 0.005 M sodium hydroxide solution using phenolphthalein indicator. The IEC = $(V_{NaOH}C_{NaOH})/M_{dry}$, where V_{NaOH} is the volume of consumed titrant (mL), C_{NaOH} is the molar concentration of titrant, and M_{dry} is the weight of the dry membrane (g).

Fourier-transform infrared (FTIR) spectra were collected using a Nicolet FTIR spectrophotometer at room temperature. Spectra were recorded using a silicon wafer as a background in the range 4000−400 cm^{-1} (see Figure S2 in the Supporting Information).

X-ray photoelectron spectroscopy (XPS) analysis were performed on a Kratos Axis Ultra X-ray photoelectron spectrometer using monochromated Al Kα radiation (1486.6 eV) at 15 kV and 10 mA (150 W). The sampling depth was up to 10 nm. Data were collected in a fixed analyzer transmission mode: Survey scans were performed from 1200−0 eV with 1.0 eV steps at an analyzer pass energy of 160 eV, and high-resolution scans were performed at 0.1 eV steps with an analyzer pass energy of 20 eV. Vision 2 software was used for data acquisition and processing including curve fitting.

Time-of-flight secondary ion mass spectrometry (ToF-SIMS) analyses were performed with a PHI model TRIFT 2100 (PHI Electronic Ltd.) spectrometer equipped with a ^{69}Ga liquid metal ion gun. A 15 kV pulsed primary ion beam was used to desorb and ionize species from the sample surface.

Simulations were carried out using the all-electron density functional theory (DFT) method implemented in DMol^3.[18] The generalized gradient approximation (GGA) was used with the Perdew−Wang exchange-correlation functional (PW91). Geometry optimization was achieved in 18 steps with an energy criterion of 10^{-4} Ha. DFT simulations were made in the microcanonical ensemble (NVE) with a target of 200 K and temperature variation of ~40 K. A time step of 1 fs was used with a thermalization of 10 ps followed by a production run of 10 ps.

RESULTS AND DISCUSSION

The QENS data, $S(Q,\omega)$, for Nafion could be described using an approximation for dispersed relaxation (in the frequency domain, equal to a stretched exponential in the time domain) proposed by Bergman[19] (see Figure S3 in the Supporting Information):

$$S(Q, \omega) = \left\{ \frac{\chi_p''}{\omega\left(1 - b + \frac{1}{1+b}\right)[b(\omega_p Q^2/\omega) + (\omega/\omega_p Q^2)^b]} \right\} \otimes R(Q, \omega) + C \quad (2)$$

where $R(Q,\omega)$ is the measured instrumental resolution function (spectrum from vanadium), C corresponds to a residual flat background, χ_p'' and ω_p define the height and position of the peak, respectively, and b is an independent shape parameter. The parameter ω_p is analogous to the more familiar width of a Lorentzian distribution. The parameter b is analogous to the stretch exponent of the exponential function in the time domain (β); for clarity, we refer to the b of the Bergman function as β. Although much of the $S(Q,\omega)$ of the PP-PEM could be fitted using the Bergman function, a broad Lorentzian function was required to capture the remaining 41(3)% of the protons that were moving more rapidly than those described using the Bergman function (see Figure S3 in the Supporting Information):

$$S(Q, \omega) = \left\{ A_1\delta(\omega = 0) + B_1\left[\frac{\chi_p''}{\omega\left(1 - b + \frac{1}{1+b}\right)[b(\omega_p Q^2/\omega) + (\omega/\omega_p Q^2)^b]} \right] + C_1\left[\frac{\Gamma}{\pi(\Gamma^2 + \omega^2)} \right] \right\} \otimes R(Q, \omega) + C \quad (3)$$

where $\delta(\omega = 0)$ is a Dirac function, the second term is the Bergman function with identical Q-dependent parameters that describe the Nafion QENS data, and the third term is a Lorentzian with half-width at half-maximum, Γ. A_1, B_1, and C_1 are the number density of scatterers associated with the Dirac, Bergman, and Lorentzian functions, respectively. C is a flat background, and b was fixed to the (Q-independent) average from the Nafion data, 0.60(7).

The Q^2 dependence of the two QENS components (Figure 2) reveals that the faster and slower-moving protons diffuse differently. For clarity, we refer to the faster and slower-moving protons as type 1 and type 2, respectively. Self-diffusion constants for the protons added in the water (D) were obtained by the approximation to Fickian diffusion achieved in the low Q region, excluding the region of confinement, where $\Delta\Gamma(Q) = DQ^2$ and $\Delta\omega_p(Q) = DQ^2$. A fit to the region where the function width increases linearly with Q^2 provides a self-diffusion constant for type 1 protons (D) of 2.8(1) × 10^{-4} cm^2 s^{-1}, this being an order of magnitude faster than the type 2 diffusion which is typical for protons in Nafion. The highest reported proton conductivity in PP-PEMs is that of PEMs produced from styrene and trifluoromethanesulfonic acid, such as those used here. The proton conductivity, measured through impedance spectroscopy,[8−10] of PP-PEMs of the same type measured here is ~21% higher than that for Nafion, supporting our findings.

The $S(Q,\omega)$ of type 2 protons in the PP-PEM was fitted with the same Bergman function used to describe the protons in the Nafion, with identical width, Q-dependency, and stretch

dx.doi.org/10.1021/jp309259k | J. Phys. Chem. C 2013, 117, 4351−4357

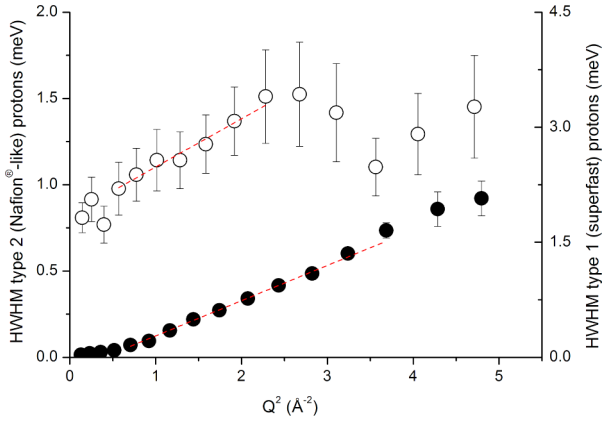

Figure 2. Q^2 dependence of the half-width at half-maximum (HWHM) for the Bergman function describing type 2 protons in the Nafion and PP-PEM (closed circles) and the Lorentian function describing type 1 protons in the PP-PEM (open circles). Dotted lines are linear fits to the region in which the HWHM broadened proportionally to DQ^2, where D is the average self-diffusion constant for the type 2 protons and the self-diffusion constant for the type 1 protons.

exponent (β). This indicates that the type 2 protons in the PP-PEM, 59(3)%, are moving in an identical way (within the limitations of the measurement) to all of the protons added to Nafion. The β of the Bergman function describing the type 2 protons is 0.61(7) and Q-independent, indicating a deviation from a Lorentzian line shape, consistent with previous QENS data for water-saturated Nafion.[11] Insights into the diffusion process can be gained by considering the variance of the displacement of protons with time, t^{β}, where normal diffusive processes are indicated by $\beta = 1$ and deviations of β from 1 indicates anomalous diffusion.[20] The β of the Bergman function describing the type 2 protons is less than 1, indicating subdiffusion processes, which may arise from correlated motions within the matrix, where the diffusing particle is confined for a time.[20] The type 1 protons in the PP-PEM are described using a Lorentzian function, and fitting with the Bergman function yields $\beta = 1$; a single-exponential decay where protons have full access to move in all dimensions. This is a different diffusion mechanism from the type 2 protons, constituting 59(3)% of protons diffusing in the PP-PEM and all protons diffusing in Nafion, where the matrix causes subdiffusive processes as a result of hindrances, which must be absent in parts of the PP-PEM. These parts correspond with the 41(3)% of type 1 protons moving through the matrix in a way that is superfast compared with the type 2 protons.

The half-width at half-maximum (HWHM) of the QENS component for the type 2 protons (in both the Nafion and the PP-PEM, Figure 2) is constant with Q^2 until $Q^2 = 0.52$ Å^{-2}. This dependency is consistent with a confined region in Nafion in which the protons diffuse.[12−14] From $Q^2 > 0.52$ Å^{-2} the width increases linearly and can be approximated by Fickian-type diffusion, yielding $D = 3.0(2) \times 10^{-5}$ cm^2 s^{-1}, which is comparable to that reported for protons in Nafion using QENS[13,14] but higher because it is for the average of the subdiffusive processes. By approximating a fit to the Nafion-like protons using a Lorentzian function, D for the type 2 protons is reduced to almost of that for fully hydrated Nafion ($2.1(1) \times 10^{-5}$ cm^2 s^{-1}).[13,14]

The temporal and spatial differences between the two proton diffusion processes, obtained directly and uniquely from the QENS data, indicate a different mechanism for the type 1 and type 2 protons. A simple following of the PP-PEM components by the water was excluded by comparing the spectrum for ^2H_2O with that for ^1H_2O (both in the PP-PEM) and demonstrating that these do not scale linearly.

The Q^2-dependent broadening of the Lorentzian function describing the type 1 protons in the PP-PEM deviates from linearity after Q^2 of ~2.5 Å^{-2} (Figure 2). This trend is characteristic for jump-diffusion, and we use the orientationally averaged Chudley−Elliott jump-diffusion model[21] to model the Q-dependent broadening (Figure 3):

$$\Delta\Gamma(Q) = \frac{1}{\tau}\left(1 - \frac{\sin(Qd)}{Qd}\right) \quad (4)$$

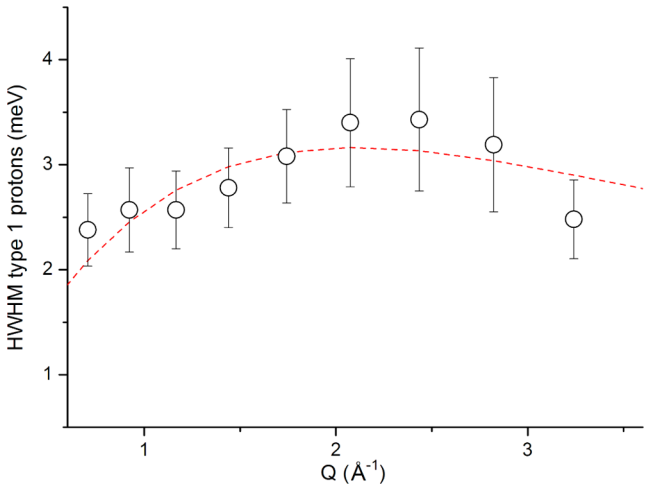

Figure 3. Q-dependence of the HWHM of the Lorentzian function describing the faster-moving protons in the PP-PEM. The dotted line is a fit of the Chudley−Elliott jump-diffusion model to the region > Q = 0.72 Å^{-1} with a jump-length of 3.1 Å and a 0.4 ps residence time, leading to a D of $1.3(2) \times 10^{-4}$ cm^2 s^{-1}.

In this model a proton has a residence time (τ) at a site before moving instantaneously to another site with a mean-square jump-length, d. D is related to d and τ: $D = d/(6\tau)$. Applying this model to the data for type 1 protons yields a jump length of ~3.1 Å and τ of 0.4 ps (Figure 3). This corresponds to $D = 1.3(2) \times 10^{-4}$ cm^2 s^{-1}, comparable with the $D = 2.8(1) \times 10^{-4}$ cm^2 s^{-1} obtained by the approximation to Fickian-type diffusion.

Neither proton conductivity (via impedance spectroscopy) nor self-diffusion (via QENS) has been studied as a function of PP-PEM hydration state, including in the present work. We measure both membranes in their water-saturated state and find that the PP-PEM investigated here has significantly less water uptake (3.0(8) wt %) than Nafion (15(1) wt %). It is noteworthy then that we measure proton diffusion in the PP-PEM that is faster than in Nafion, as proton diffusion in Nafion is hydration-dependent with both local and long-range proton self-diffusion constants increasing with hydration.[14] Proton conduction in Nafion is strongly linked to hydration,[22] with Nafion nanostructure linked to water dynamics in simulations that agree with QENS results.[14,23] The orientational diffusion of molecules within Nafion is also linked to hydration.[24] Further, PP-PEMs are reported to have a disorganized and highly cross-linked structure, leading to a lower intrinsic permeability of

dx.doi.org/10.1021/jp309259k | J. Phys. Chem. C 2013, 117, 4351−4357

methanol compared with that of Nafion. This enables a reduction of the methanol crossover in PP-PEMs, with PP-PEMs exhibiting a methanol permeability 10 times less[3,4,8,9] or lower[10] than for Nafion. Consequently, these PP-PEMs are being pursued for use in direct methanol fuel cell applications.

The type 1 diffusion process in the PP-PEM circumvents the limitations of the type 2 diffusion in Nafion, with the important variables likely to be the density and arrangement of the proton conduction groups. We measure sulfonate concentration and species using X-ray photoelectron-spectroscopy (XPS) and time-of-flight secondary-ion mass spectrometry (ToF-SIMS) (see Figure 4 and Figures S4 and S5, respectively). In the PP-PEM the proton-conductive functions are derived from the trifluoromethanesulfonic acid.[3,4,8−10] Tof-SIMS results were normalized to PEM carbon content and indicated similar trends for the amount of sulfur and oxygen to XPS results. XPS results are reported from an average of 10 measurement points and were highly reproducible, indicating a compositionally homogeneous PEM. In the pulsed-plasma method, deposition occurs in the "off" period and fragmentation in the "on" period; Tof-SIMS of our PP-PEMs reveals a sulfonate concentration that depends on the pulsed-plasma duty cycle (% "on" time; see Figures S4 and S5). PP-PEMs from a 10% and 50% duty cycle and 10 ms pulse time have higher concentrations of sulfonate than Nafion, ≈8.6% and 5.6%, respectively, relative to ≈1.8% for Nafion. These results agree with the 4.8% and up to 5% sulfonates found previously in similar PP-PEMs.[4,8−10] The QENS data were obtained for PP-PEMs made with a 68 ms pulse time and an 11.7% duty cycle. The acid in these membranes was estimated through IEC measurements and was 0.7 mequiv g^{-1} for the PP-PEM, an amount comparable to that measured here for Nafion (~0.91 mequiv g^{-1}). It follows that differences between the type 1 and 2 proton diffusion are not due to more sulfonate but from differences in sulfur environment.

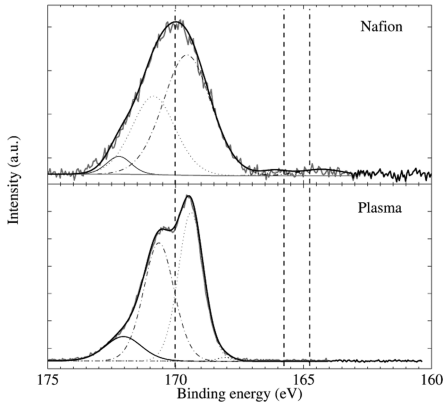

Figure 4. High-resolution XPS sulfur spectrum for Nafion (top) and the PP-PEM (bottom).

XPS spectra indicate differences in the local environment of the sulfur in Nafion and the PP-PEM. The sulfur spectra for both PEMs can be fitted by three peaks at binding energies of approximately 169.2, 170.6, and 171.9 eV (Figure 4), indicating that the dominant sulfur peaks are in the form of sulfonic acid. The spectrum that we obtain for the PP-PEM features a clear splitting of these S2p components that is not present in the Nafion spectrum. Hence, although the Nafion spectrum displays SO_2 and SO components, the PP-PEM does not, indicating a high retention of the SO_3 group in the PP-PEM.

The ToF-SIMS results show that the complete $CF_3SO_3^-$ anion is detected in the PP-PEM and not in Nafion and that the $CF_3SO_3^-$ species accounts for ~11% of the total negative ion spectrum for the PP-PEM compared with ~0.05% for Nafion (see Figures S4 and S5). The SO_3 components comprise ~0.4% of the total negative ion spectrum for the PP-PEM and ~3.5% for Nafion. The S2p spectrum for the PP-PEM is very similar to that obtained previously for the PP-PEM with the highest reported conductivity.[8−10] Taken together, the XPS and Tof-SIMS analyses indicate a high retention of SO_3 groups with the dominant sulfur-containing environment in the PP-PEM to be unpolymerized trifluoromethanesulfonic acid.

Hydrates of trifluoromethanesulfonic acid provide model systems for understanding proton transport in PEMs, with studies revealing that proton transfer is influenced by the proximity of sulfonates.[25] Diffusion of triflic acid and triflate/water mixtures is less than 1×10^{-5} $cm^2\ s^{-1}$, less than for protons in either PEM studied here.[26] This indicates that although the PP-PEM does contain free triflic acid, the proton diffusion mechanism arises from the membrane itself, perhaps in conjunction with the triflic acid (Figure 5).

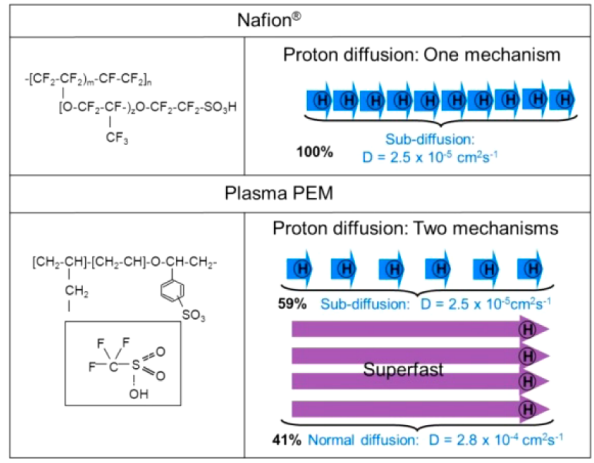

Figure 5. Summary of chemical structure (left) and proton self-diffusion mechanism (right) for Nafion (top) and the PP-PEM (bottom).

The arrangement of sulfonates in the PP-PEM is probably key to enabling the superfast diffusion. This theory is further supported by the fact that the PP-PEM studied here has the fastest reported proton self-diffusion for any PEM and contains a similar local environment of the sulfur-containing groups (similar XPS spectra) to the PP-PEM with the highest reported conductivity.[8−10] Furthermore, we note that the plasma-production method of the PP-PEM studied here and that with the highest reported proton conductivity[8−10] are also very similar. Specifically, both PP-PEMs are made in similarly designed reactors, using a capacitive source, with precursors that are carried into the reaction region under the source production region, with the same rf drive frequency, and under similar pressure. Similarly, the concentration of triflic acid is likely to play a role in determining the local structure of sulfonates within the PP-PEM and therefore to affect the proton conduction.

dx.doi.org/10.1021/jp309259k | J. Phys. Chem. C 2013, 117, 4351−4357

The proton self-diffusion results that we present for Nafion (Figure 5) are in agreement with previous work.[11−14] Knowledge of the structure of proton conductive groups in Nafion has led to a further understanding of the proton conduction mechanisms through molecular dynamics simulations[23] validated against previous QENS data.[14] Despite these and other efforts, the exact mechanism of proton conduction in Nafion is not fully understood, partly as a result of its complex structure, which is also not fully known. Much more is known about the structure of Nafion than the PP-PEM, and in the absence of structural knowledge regarding the proton-conducting parts of the PP-PEM, we cannot propose a detailed mechanism for either of the proton diffusion processes in the PP-PEM.

Nevertheless, there are notable differences between the type 1 and 2 proton diffusion, and to investigate the plausibility of the relatively long (3.1 Å) jump distance for the type 1 process obtained from QENS, we constructed a simple model in which a hydronium ion (in reality probably solvated) passes between two trifluoromethanesulfonates in an operation that relates the two proton sites at ≈2.5 Å. The potential energy of the model was minimized by bringing the two sulfonates and the hydronium ion into proximity and allowing all atoms to move until the forces acting on them were zero; the result was used as a starting model for a molecular dynamics (MD) simulation. During this simulation the positions of the two carbon atoms were fixed to prevent the model from exploring physically unreasonable states, and we note that the motions of the two SO_3^- ions assisted the proton transfer between them with a transfer distance of ≈2.4 Å. Although this distance is shorter than the 3.1 Å derived from QENS, a picture of local environments of trifluoromethanesulfonate emerges for the PP-PEM, whose dynamics assist proton transfer over relatively long jump distances. The local environments that allow these fast proton dynamics are absent in Nafion.

In the absence of more detailed structural information, it is difficult to justify a more detailed model, and using this simple model, we show that assisted superfast diffusion is possible using an analysis of the separation and position of the atoms in the hydrogen-bonded water bridge formed between two trifluoromethanesulfonate groups. This analysis reveals a concerted process in which the three hydronium O−H distances vary between 0.85 and 1.175 Å—the shorter lengths arising when a H is associated more with the water and the longer lengths arising as the atom approaches a sulfonate oxygen (SO) more closely. The situation in which two H atoms of the hydronium ion can associate closely with two oxygen atoms on separate trifluoromethanesulfonate groups simultaneously can be understood by a straightforward analysis of the correlation between the r(SO···H) and the shortest distance between two O atoms on different trifluoromethanesulfonate groups, r(SO···OS). The two-dimensional frequency distribution is shown in Figure 6. The island of intensity at r(SO···H) = 1.27 Å corresponds to a H atom being on the "chosen" trifluoromethanesulfonate group, while the intensity at 1.72 Å corresponds to a H atom being on the "other" trifluoromethanesulfonate group. These arise at SO···OS separations of 4.7−4.8 Å, and at this separation there is also intensity at r(SO···H) between 1.50 and 1.65 Å, corresponding to the existence of an almost symmetric H_3O^+ between the two sulfonates. The intensity at r(SO···H) = 1.35 Å arises at the comparatively short r(SO···OS) of 4.52 Å, reflecting a H_3O^+ that is symmetrically shared between the two trifluoromethanesulfonate groups.

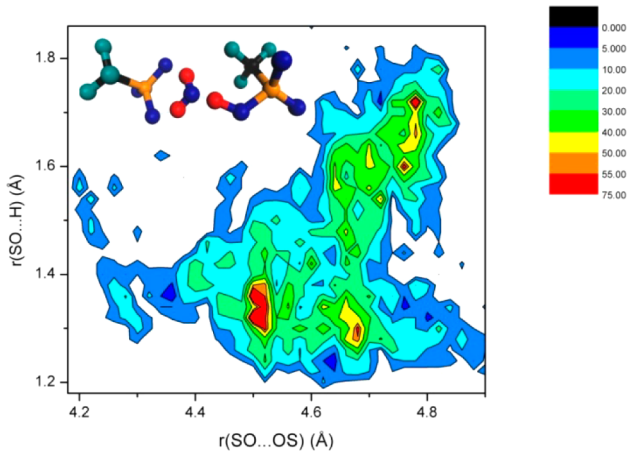

Figure 6. Two-dimensional frequency distribution of the distance between any hydrogen and a given trifluoromethanesulfonate oxygen, r(SO···H), and the separation distance between two oxygen atoms on separate trifluoromethanesulfonate groups, r(SO···OS). The model is shown in the inset (where sulfur is orange, carbon is gray, oxygen is blue, fluorine is turquoise, and hydrogen is red). The analysis is over 10 000 molecular dynamics 1 fs frames. Intensity is shown in the legend.

While proton transfer does not occur each time that this symmetric sharing occurs, it is always the precursor to a successful transfer process.

CONCLUSIONS

Ionically conductive films prepared by plasma polymerization hold many advantages for microfuel cell applications, and we directly measure proton self-diffusion in a plasma-polymerized PEM that is an order of magnitude faster than in Nafion. Our experiments suggest that the plasma production provides local arrangements of trifluoromethanesulfonate that enable an assisted diffusion process. This work demonstrates that a leap in PEM performance is possibl, however, it is important to determine the arrangement of proton conducting groups as well as both short- and long-range structure of the plasma-polymerized PEM to understand the details of the mechanism by which the superfast diffusion occurs. The plasma method enables the direct and rapid control of the membrane's chemical composition and microstructure which will enable these characteristics to be adjusted for permeability and both chemical and thermal stability as well as to better exploit the superfast diffusion.

ASSOCIATED CONTENT

Supporting Information

XPS carbon and FTIR spectra, fitted QENS spectra, and Tof-SIMS results. This material is available free of charge via the Internet at http://pubs.acs.org.

AUTHOR INFORMATION

Corresponding Author

*E-mail vanessa.peterson@ansto.gov.au, Tel +61 2 9717 9401.

Present Address

‖ESS-Bilbao, UPV/EHU Edif. rectorado, Leioa, Spain.

Notes

The authors declare no competing financial interest.

■ ACKNOWLEDGMENTS

We thank Dr. Margarita Russina for support of the NEAT spectrometer at the Berlin Neutron Scattering Center where QENS data were measured. We also acknowledge the technical, scientific, and financial assistance from the Australian Microscopy and Microanalysis Research Facility for the ToF-SIMS and XPS measurements.

■ ABBREVIATIONS

PP-PEM, plasma-polymerized PEM; QENS, quasielastic neutron scattering.

■ REFERENCES

(1) Mauritz, K. A.; Moore, R. B. State of Understanding of Nafion. *Chem. Rev.* **2004**, *104*, 4535−4585.
(2) Dupius, A. C. Proton Exchange Membranes for Fuel Cells Operated at Medium Temperatures: Materials and Experimental Techniques. *Prog. Mater. Sci.* **2011**, *56*, 289−327.
(3) Ennajdaoui, A.; Roualdes, S.; Brault, P.; Durand, J. Membranes Produced by Plasma Enhanced Chemical Vapor Deposition Technique for Low Temperature Fuel Cell Applications. *J. Power Sources* **2010**, *195*, 232−238.
(4) Roualdes, S.; Topala, I.; Mahdjoub, H.; Rouessac, V.; Sistat, P.; Durand, J. Sulfonated Polystyrene-Type Plasma-Polymerized Membranes for Miniature Direct Methanol Fuel Cells. *J. Power Sources* **2006**, *158*, 1270−1281.
(5) Leich, M. A.; Mackie, N. M.; Williams, K. L.; Fisher, E. R. Pulsed Plasma Polymerization of Benzaldehyde for Retention of the Aldehyde Functional Group. *Macromolecules* **1998**, *31*, 7618−7626.
(6) Fraser, S.; Short, R. D.; Barton, D.; Bradley, J. W. A Multi-Technique Investigation of the Pulsed Plasma and Plasma Polymers of Acrylic Acid: Millisecond Pulse Regime. *J. Phys. Chem. B* **2002**, *106*, 5596−5603.
(7) Groenewoud, L. M. H.; Engbers, G. H. M.; Terlingen, J. G. A.; Wormeester, H.; Feijen, J. Pulsed Plasma Polymerization of Thiophene. *Langmuir* **2000**, *16*, 6278−6286.
(8) Jiang, Z. Q.; Jiang, Z. J.; Yu, X. Y.; Meng, Y. D. Preparation of Proton Exchange Membranes by a Plasma Polymerization Method and Application in Direct Methanol Fuel Cells (DMFCs). *Plasma Process. Polym.* **2010**, *7*, 382−389.
(9) Jiang, Z. Q.; Jiang, Z. J. Preparation of Proton Exchange Membranes with High Performance by a Pulsed Plasma Enhanced Chemical Vapor Deposition Technique (PPECVD). *RSC Adv.* **2012**, *2*, 2743−2747.
(10) Jiang, Z. Q.; Jiang, Z. J.; Meng, Y. D. Optimization and Synthesis of Plasma Polymerized Proton Exchange Membranes for Direct Methanol Fuel Cells. *J. Membr. Sci.* **2011**, *372*, 303−313.
(11) Volino, F.; Pineri, M.; Dianoux, A. J.; De Geyer, A. Water Mobility in a Water-Soaked Nafion® Membrane: A High-Resolution Neutron Quasielastic Study. *J. Polym. Sci., Polym. Phys. Ed.* **1982**, *20*, 481−496.
(12) Paciaroni, A.; Casciola, M.; Cornicchi, E.; Marconi, M.; Onori, G.; Pica, M.; Narducci, R. Temperature-Dependent Dynamics of Water Confined in Nafion Membranes. *J. Phys. Chem. B* **2006**, *110*, 13769−13776.
(13) Perrin, J. C.; Lyonnard, S.; Volino, F. Quasielastic Neutron Scattering Study of Water Dynamics in Hydrated Nafion Membranes. *J. Phys. Chem. C* **2007**, *111*, 3393−3404.
(14) Pivovar, A. A.; Pivovar, B. S. Dynamic Behavior of Water within a Polymer Electrolyte Fuel Cell Membrane at Low Hydration Levels. *J. Phys. Chem. B* **2005**, *109*, 785−793.
(15) Lyonnard, S.; Berrod, Q.; Brüning, B.-A.; Gebel, G.; Guillermo, A.; Ftouni, H.; Ollivier, J.; Frick, B. Perfluorinated Surfactants as Model Charged Systems for Understanding the Effect of Confinement on Proton Transport and Water Mobility in Fuel Cell Membranes. A Study by QENS. *Eur. Phys. J. Spec. Top.* **2010**, *189*, 205−216.
(16) Rollet, A.-L.; Simonin, J. P.; Turq, P.; Gebel, G.; Kahn, R.; Vandais, A.; Noell, J.-P.; Malveau, C.; Canet, D. Self-Diffusion of Ions at Different Time Scales in a Porous and Charged Medium: The Nafion Membrane. *J. Phys Chem B* **2001**, *105*, 4503−4509.
(17) Page, K. A.; Park, J. K.; Moore, R. B.; Garcia Sakai, V. Direct Analysis of the Ion-Hopping Process Associated with the α-Relaxation in Perfluorosulfonate Ionomers Using Quasielastic Neutron Scattering. *Macromolecules* **2009**, *42*, 2729−2736.
(18) Delley, B. From Molecules to Solids with the DMol3 Approach. *J. Chem. Phys.* **2000**, *113*, 7756−7764.
(19) Bergman, R. General Susceptibility Functions for Relaxations in Disordered Systems. *J. Appl. Phys.* **2000**, *88*, 1356−1365.
(20) Jobic, H.; Theodorou, D. N. Quasi-elastic Neutron Scattering and Molecular Dynamics Simulation as Complementary Techniques for Studying Diffusion in Zeolites. *Microporous Mesoporous Mater.* **2007**, *102*, 21−50.
(21) Chudley, C. T.; Elliott, R. J. Neutron Scattering from a Liquid on a Jump Diffusion Model. *Proc. Phys. Soc. London* **1961**, *77*, 353−361.
(22) Paddison, S. J. Proton Conduction Mechanisms at Low Degrees of Hydration in Sulfonic Acid-Based Polymer Electrolyte Membranes. *Annu. Rev. Mater. Res.* **2003**, *33*, 289−319.
(23) Devanathan, R.; Venkatnathan, D.; Dupuis, M. Atomistic Simulation of Nafion Membrane. 2. Dynamics of Water Molecules and Hydronium Ions. *J. Phys. Chem. B* **2007**, *111*, 13006−13016.
(24) Spry, D. B.; Goun, A.; Glusac, K.; Moilanen, D. E.; Fayer, M. D. Proton Transport and the Water Environment in Nafion Fuel Cell Membranes and AOT Reverse Micelles. *J. Am. Chem. Soc.* **2007**, *129*, 8122−8130.
(25) Hayes, R. L.; Paddison, S. J.; Tuckerman, M. E. Proton Transport in Triflic Acid Hydrates Studied via Path Integral Car-Parrinello Molecular Dynamics. *J. Phys. Chem. B* **2009**, *113*, 16574−16589.
(26) Sunda, A. P.; Venkatnathan, A. Molecular Dynamics Simulations of Triflic Acid and Triflate Ion/Water Mixtures: A Proton Conducting Electrolytic Component in Fuel Cells. *J. Comput. Chem.* **2011**, *32*, 3319−3328.